ELSEVIER

Ceramics International 28 (2002) 467–477

CERAMICS INTERNATIONAL

www.elsevier.com/locate/ceramint

Electrochemical synthesis of nanocrystalline $CoFe_2O_4$ thin films and their characterization

S.D. Sartale, C.D. Lokhande*

Thin Film Physics Laboratory, Department of Physics, Shivaji University, Kolhapur- 416 004 (M.S.), India

Received 18 April 2001; received in revised form 8 June 2001; accepted 3 October 2001

Abstract

The electrochemical oxidation (anodization) of electrodeposited $CoFe_2$ alloy films in alkaline solution (1 N KOH) is depicted as a novel and powerful route for preparing spinel nanocrystalline $CoFe_2O_4$ thin films. $CoFe_2$ alloy films were electrodeposited from simple aqueous sulphate bath. Several key processing parameters were optimized to obtain good quality $CoFe_2$ alloy films with maximum thickness. The films resulting from electrochemical oxidation for 30 min at 5 mA/cm^2 current density possess high quality surface and well crystallized spinel cubic $CoFe_2O_4$ structure. The effects of air annealing of electrochemically oxidized alloy films on various properties were studied.

Keywords: C. Magnetic properties; Nanocrystalline $CoFe_2O_4$ thin films; Electrosynthesis; Crystal structure; Surface morphology

1. Introduction

$CoFe_2O_4$ possesses the so-called inverse spinel structure with one half of Fe^{3+} ions on A site and the rest, together with Co^{2+} ions, on B sites at room temperature. The cation distribution depends on the thermal history of the samples [1,2]. $CoFe_2O_4$ in bulk and thin film form has attracted considerable attention for its fundamental understanding and large scale technological applications as transformer cores, recording heads, antenna rods, loading coils, memory, microwave devices, catalyst, ferrofluids, magnetic refrigeration, solar energy conversion into H_2 and biomedical applications and sensors [3–8]. Thin films of $CoFe_2O_4$ are very promising materials for magneto–optical recording and thin film device applications due to their physical properties such as high recording density, high coercivity, moderate saturation magnetization, chemical stability and mechanical hardness [9–13].

Thin films of $CoFe_2O_4$ have been prepared by several techniques such as laser deposition, sputtering, ion-beam deposition, sol–gel deposition, spray pyrolysis, ferrite plating and electroless deposition [14–22]. All these methods require substrate heating during and/or after deposition of the film, which imposes restrictions on selection of the substrate material and does not allow the deposition on devices (e.g. GaAs integrated circuits), which might degenerate by exposure to high temperature. Also, the particles obtained by these processes are rather large and nonuniform in size.

The electrochemical (processes) route is an attractive alternative to some of the other deposition techniques in order to overcome shortcomings due to high deposition temperature. The advantage of the electrochemical route is not only the lower deposition temperature but also the small grain size of the deposit obtained, which is required for high-density magneto–optic recording media [19]. Since the electrochemical route is a room temperature technique, it prevents the inhalation of toxic gases produced at high temperature during processing. Thus, the electrochemical route is not only interesting as a field of study of chemical reactions but also as an environmental friendly process.

Electrochemical oxidation at room temperature in alkaline solution (1 N KOH or NaOH) has been used to prepare highly oxidized ferrite [23]. For the first time [24,25], we have reported room temperature preparation of $CuFe_2O_4$ and $NiFe_2O_4$ thin films from aqueous medium using electrochemical route. The method proceeds into two steps: first the electrodeposition of MFe_2 (M = divalent metal ion) alloy films and their sub-

* Corresponding author. Tel.: +91-0231-690571; fax: +91-0231-690533.

E-mail address: l_chandrakant@yahoo.com (C.D. Lokhande).

0272-8842/02/$22.00
PII: S0272-8842(01)00119-5

sequent electrochemical oxidation (anodization) in aqueous 1 N KOH electrolyte to intercalate oxygen species into alloy films. In the present investigation, an attempt is made to deposit $CoFe_2O_4$ thin films using electrochemical route.

Electrodeposition of iron group metal (Co, Ni and Fe) alloys is one of the most important developments in the metal and/or alloy deposition field. These alloys have potential applications in the sophisticated electronics industries related to computers, rocketry, space technology, automotive industries, energy storage devices, etc. [26]. The iron group metals are inert with high overpotential, low exchange current density and low hydrogen overpotential [27]. Electrodeposition of binary alloys of the iron group metals exhibits the phenomenon known as anomalous codeposition [28]. In the anomalous codeposition, the less noble metal deposits preferentially; consequently, its relative content in the alloy deposit is much higher than in the solution. Another important factor, which influences the kinetics, composition and properties of electrodeposited iron group metal alloys is simultaneous hydrogen evolution [29]. Numerous studies focusing upon the effects of additives, the presence of O_2, the inclusion of higher oxidation state of metals (M^{3+}) in the plating solution and differences in the anions have been conducted for a better understanding of iron-group electrodeposition and several hypotheses have been presented in the literature [30–37].

In this report, deposition of $CoFe_2O_4$ thin films onto different conducting substrates from aqueous medium using electrochemical route is described. The different processing parameters such as deposition potential, current density, deposition period and bath temperature are optimized and reported to get good quality $CoFe_2$ alloy films with maximum thickness. Compositional analyses of alloy films were done using atomic absorption spectroscopy (AAS) technique. Anodization conditions such as current density and period are optimized to get good quality $CoFe_2O_4$ thin films. Effect of air annealing on various properties is also studied. Structural changes of alloy films due to anodization and annealing were studied by X-ray powder diffraction (XRD) technique. Morphological and microstructural information of the films was obtained using optical microscopy and scanning electron microscopy (SEM) techniques. Magnetic properties of $CoFe_2O_4$ films were measured with fully automated vibrating sample magnetometer (VSM) technique.

2. Experimental details

2.1. Synthesis

2.1.1. Electrolyte bath

Analar reagent grade (impurity of the order of 10^{-3}%) chemicals [cobalt sulphate ($CoSO_4{\cdot}7H_2O$), ferrous Sulphate ($FeSO_4{\cdot}7H_2O$) and potassium hydroxide (KOH)] supplied by Loba Chemie, India were used for bath preparation. Requisite amounts of chemicals were weighed accurately and dissolved in double distilled water to obtain the desired bath concentration. All solutions were prepared immediately prior to each deposition. The bath was kept unstirred and at constant desired temperature.

2.1.2. Substrates

Thin plates (thickness ~2–3 mm) of stainless steel, copper and titanium and fluorine doped tin oxide (FTO) coated glass (sheet resistance ~10–20 Ω cm^2) were used as cathode substrates. The backside of the metal substrates was covered with insulating tape. The cathode deposition area was between 1 to 4 cm^2. The metal substrates were mirror polished with zero grade polish paper, cleaned with detergent, ultrasonically cleaned in double distilled water, rinsed with acetone and methanol and dried with hot air. The FTO coated glass substrates were cleaned using 50% dilute HCl, ultrasonically cleaned in double distilled water, rinsed with acetone and methanol and dried with hot air. Just before the deposition each substrate was anodically etched at a constant current density 10 mA/cm^2 for 1 min in the bath similar to that used for deposition.

2.1.3. Alloy electrodeposition

The electrodeposition of Co–Fe alloy films was carried out from an electrolyte bath consisting 0.05 M $CoSO_4$ and 0.1 M $FeSO_4$ aqueous solutions in various proportions. The distance between anode and cathode was 0.5 cm. High quality graphite was used as an anode. The electrodeposition was carried out under galvanostatic mode using constant current source (0–200 mA). All potentials were measured with reference to saturated calomel electrode (SCE), whose tip was located within 2 cm from the cathode. Deposition potentials of metals and alloy were determined by plotting cathodic polarization curves. Influence of bath composition, substrate and bath temperature on deposition potentials of metals and alloy was studied. Bath composition for alloy deposition was optimized by the atomic weight percentage of Fe in the deposit determined by AAS technique. Several processing parameters were optimized in order to get good quality $CoFe_2$ alloy films with maximum thickness. The optimized preparative parameters are summarized in Table 1. The good quality of the films was tested by observing deposit surface (uniformity) and adherence test (tape test). After deposition films were washed with double distilled water and preserved in dessicator.

The partial currents of alloy components were calculated from the mass (measured using microbalance), composition of Co and Fe (~34 and ~66%) in the deposited alloy (determined using AAS technique) and the electrolysis charge passed using Faraday's law. The

Table 1
Optimized preparative parameters for electrodeposition and anodization of $CoFe_2$ alloy films

I Electrodeposition	
(a) Bath composition:	(10 cc) 0.05 M $CoSO_4$ + (10 cc) 0.1 M $FeSO_4$
(b) Current density:	7 mA/cm^2
(c) Deposition time:	20 min.
(d) Bath temperature:	room temperature (27 °C)
II Anodization	
(a) Electrolyte:	1 N KOH
(b) Current density:	10 mA/cm^2
(c) Intercalation time:	20 min
(d) Electrolyte temperature:	room temperature (27 °C)

current of the side reactions was obtained by subtracting the metal partial currents from the total current. It was assumed that a part of total current employed for alloy deposition was used for hydrogen evolution from the reduction of protons (H^+) and dissociation of water molecules.

2.1.4. Alloy anodization

The alloy films were electrochemically oxidized (anodized) at room temperature (27 °C). The $CoFe_2$ alloy film acts as an anode while the graphite as a cathode. KOH (1 N) aqueous solution was used as an electrolyte to intercalate oxygen species into $CoFe_2$ alloy films to form $CoFe_2O_4$. Electrochemical reactions were carried out at steady current. The oxygen evolution is occurring at higher anodic potential (>0.7V vs. SCE) according to the following reaction [23]:

$$4OH^- \rightarrow O_2 \uparrow + 2H_2O + 4e^- \quad (1)$$

The above reaction is the signature of the oxidation process of the alloy, which can be written as follows:

$$CoFe_2 + 8OH^- \rightarrow CoFe_2O_4 + 4H_2O + 8e^- \quad (2)$$

The oxidation conditions (current density and time) were optimized such that after oxidation the films will be adherent to the substrate. It was observed that oxidation at 5 mA/cm^2 current density for 30 min results into well adherent oxide films. Further increase in current density or time causes peeling of the film from the substrate. After oxidation, the films were washed with double distilled water and further characterizations were carried out.

2.1.5. Air annealing

Freshly deposited films may contain many defects such as voids, pinhole, etc. Annealing in air or vacuum reduces the defects and increases grain size. The electrochemically oxidized films onto various substrates were annealed in air for different temperatures and time periods. It was observed that above 500 °C, due to thermal mismatch between film and substrate, the films peel off from the substrate. For 5 h annealing, the films onto various substrates were well adherent to the substrates. The films were annealed in air at 500 °C temperature for 5 h and slow cooled in a furnace to room temperature. The object of this air annealing was to complete the desired physical and chemical processes.

2.2. Characterization

2.2.1. Alloy film composition

The compositional analyses of Co–Fe alloy films were carried out using atomic absorption spectroscopy (AAS) technique with Perkin-Elmer model 3030B spectrometer. Typically solutions were analyzed in the concentration range 1–5 ppm using four standards. The uncertainty in the measurement was ±3% for analytical analysis of the solution concentration.

Following the deposition, the Co–Fe alloy films were dissolved in nitric acid. The resulting solutions were diluted to a known volume in the preparation of atomic absorption spectroscopy measurement. Nitric acid was determined not to cause interference for atomic absorption spectra measurements of iron group metals.

2.2.2. Film thickness

$CoFe_2$ alloy film thickness was determined by the method of gravemetric weight difference in which area and weight of the film are measured. Before and after alloy deposition onto stainless steel substrates, the films were precisely weighed; the difference of two masses gives the mass of alloy films. The thickness was obtained by assuming the density of bulk $CoFe_2$ expressed as:

$$\rho = \rho_1 x_1 + \rho_2 x_2 \quad (3)$$

where ρ_1, ρ_2 and x_1, x_2 are densities and atomic fractions of Co (0.34%) and Fe (0.66%) elements in alloy, respectively. By putting the values of densities of Co and Fe [38], the density of $CoFe_2$ alloy is found to be 8.203 g/cc.

2.2.3. Crystal structure

The structural characterizations of alloy and oxide films onto various substrates were carried out using X-ray diffraction technique. The X-ray diffraction data of films were obtained on microcomputer controlled Philips PW3710 X-ray diffractometer with a copper anticathode without monochromator using CuK_α radiations operated at 25 kV and 20 mA. Measurements were made at 0.020° intervals of 2θ over the range 10–100° with a count time of 0.25 s for each step. The patterns were taken with zero background intensity using software facility available with the diffractometer. The grain size of the deposits was estimated from the full width at

half maximum (FWHM) of the most intense diffraction line using Scherrer's equation.

The infrared spectra of oxide film powders were recorded using Perkin-Elmer infrared spectrophotometer model 783 in the spectral range 200–800 cm^{-1}. The pellets were prepared by mixing KBr with the oxide powder collected by scratching from the stainless steel substrate in the ratio 300:1 and then pressing powder between two pieces of polished stainless steel. The pellet holder was placed on the spectrophotometer and the spectrum was scanned in the range 200–800 cm^{-1}. The noise in the range 200–300 cm^{-1} is due to CO_2 and moisture in air and hence not considered.

2.2.4. Surface morphology and microstructure

Surface morphology of alloy and oxide films deposited onto FTO coated glass substrates was studied using Orthoplan optical microscope (Leitz, Germany). The observations were made with 160× magnification in transmission mode.

Microstructure of alloy and oxide films onto stainless steel substrates was analyzed using scanning electron microscopy (SEM) technique. The as-deposited films may have overgrowth and hence micrographs were taken of the films etched in 1% HCl for 1 min. The films were coated with gold palladium by a Polaron sputtering unit. The coating thickness was 10 nm. A Cambridge MK-3 instrument with 20 keV electron beam acceleration voltage was used to take SEM images.

3. Results and discussion

3.1. Bath composition

At room temperature (27 °C) Co–Fe alloy was galvanostatically electrodeposited from the bath made by mixing 0.05 M $CoSO_4$ and 0.1 M $FeSO_4$ aqueous solutions in different volume ratios, keeping the total quantity the same (20 cc). The deposition was carried out onto stainless steel substrates at 7 mA/cm^2 current density for 20 min. Fig. 1 shows the plot of amount of Fe in the deposited alloy with volume of 0.1 M $FeSO_4$ solution in the bath. It is observed that for (10 cc) 0.05 M $CoSO_4$ + (10 cc) 0.1 M $FeSO_4$ bath solution the deposited alloy has ~34% Co and ~66% Fe composition, suggesting anomalous behaviour of the codeposition. Therefore, (10 cc) 0.05 M $CoSO_4$ + (10 cc) 0.1 M $FeSO_4$ bath was used for further studies.

3.2. Deposition potential

Polarization curves for the deposition of pure metals from a solution of given concentrations are used rather frequently in estimating the possibility of preparing an alloy, or even in obtaining a rough idea as to the composition of this alloy. It is clear that electrodeposition from these solutions is through anion discharge. The discharge of anions under these conditions is strongly dependent on the charge of the surface on which the discharge is taking place. At the same time, it is natural to expect that the null-charge of the electrode would be strongly dependent on the alloy composition. It is clear that these are the principle factors determining the position of the total polarization curve for deposition of the alloy. This curve frequently falls between the polarization curves for individual metals at more negative potentials than the curve for the more noble metal. Therefore, for simultaneous codeposition of metals, the deposition potential of alloy should be such that the deposition potentials of individual metals come closer to each other and the resultant alloy deposit will uniform, dense and well adherent to the substrate.

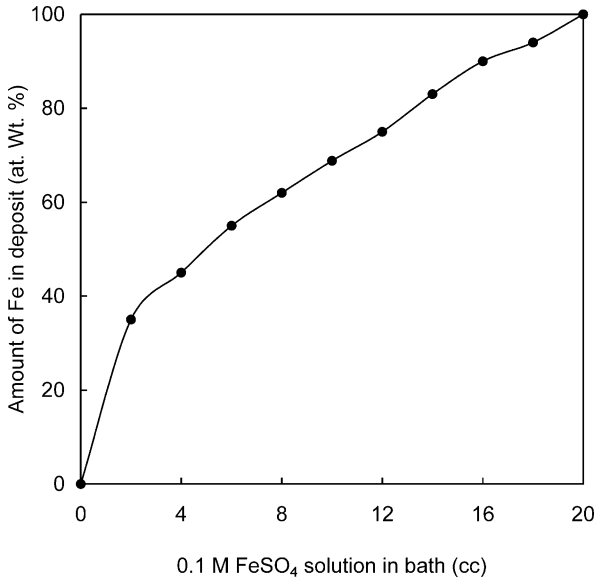

Fig. 1. Plot of amount of Fe in the deposited alloy with volume of 0.1 M $FeSO_4$ solution in the bath.

Figs. 2 and 3 show the cathodic polarization curves for reduction of $CoFe_2$ alloy at room temperature (27 °C) onto different substrates and for different bath temperatures onto stainless steel substrate from (10 cc) 0.05 M $CoSO_4$ + (10 cc) 0.1 M $FeSO_4$ bath, respectively. The estimated deposition potentials of metals and alloy for different substrates and bath temperature are noted in Table 2. In all cases, hydrogen evolution was observed above the estimated deposition potential during deposition, resulted into non-homogeneous film formation. It is seen that deposition potential of $CoFe_2$ alloy is in between deposition potentials of Co and Fe for different substrates at different temperatures. This may be due to the fact that deposition of more noble metal ions can take place at lower potential, when it is a constituent metal of the alloy getting deposited with another less noble metal ion [39]. Different deposition

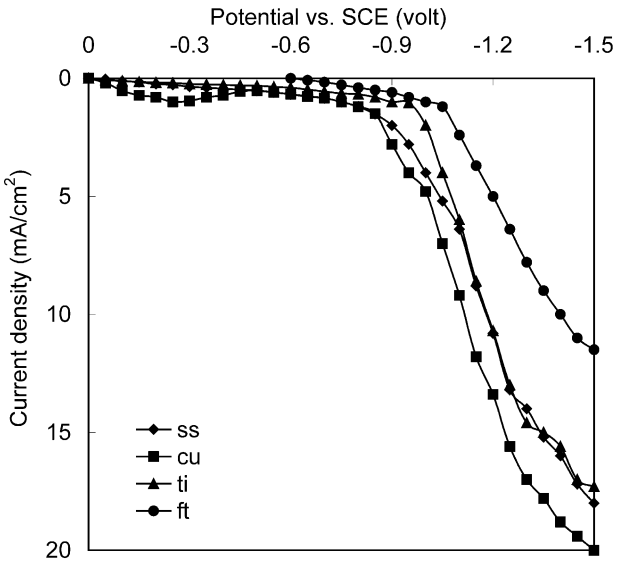

Fig. 2. Polarization curves for reduction of $CoFe_2$ alloy from (10 cc) 0.05 M $CoSO_4$ + (10 cc) 0.1 M $FeSO_4$ solution onto different substrates: ss, stainless steel, cu, copper; ti, titanium; ft, FTO coated glass at room temperature.

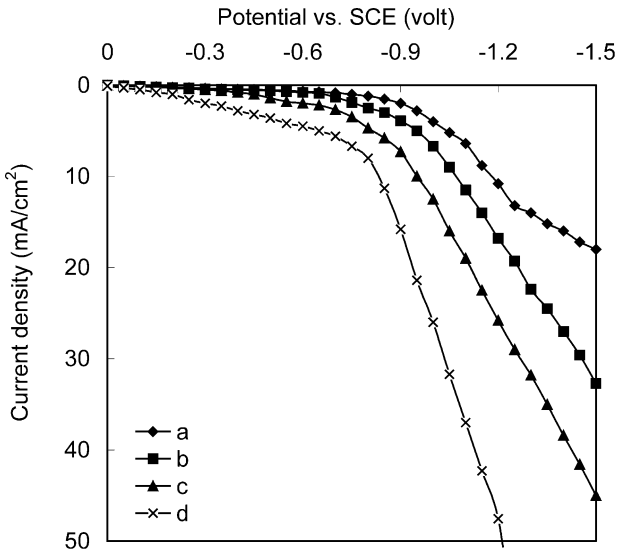

Fig. 3. Polarization curves for reduction of $CoFe_2$ alloy from (10 cc) 0.05 M $CoSO_4$ + (10 cc) 0.1 M $FeSO_4$ solution onto stainless steel substrate at (a) 30, (b) 50, (c) 70 and (d) 90 °C bath temperatures.

potentials of metals and alloy for different substrates may be due to polycrystalline substrates (evidenced by XRD study) and the orientation of planes are varying from substrate to substrate. Thus, the order of mismatching between the deposited material and substrate gives different values of deposition potentials. Also, the affinity of the substrate material is different for different depositing material [40]. It is also seen that as the bath temperature increases the deposition potential decreases. Generally a rise in bath temperature increases the grain size of the deposited material and increase in the grain size results in a decrease in the deposition potential. Additionally, the rise in bath temperature enhances the rate of diffusion and the ionic mobility and hence the conductivity of the deposition bath. Also, the decrease in deposition potential might be due to increase in the content of more noble metal (cobalt) in the deposited alloy [28].

3.3. $CoFe_2$ alloy film thickness

Thickness is the single most significant film parameter. $CoFe_2$ alloy films were deposited onto stainless steel substrates from (10 cc) 0.05 M $CoSO_4$ + (10 cc) 0.1 M $FeSO_4$ bath were used for thickness measurements. Influence of current density, deposition time and bath temperature on $CoFe_2$ alloy film thickness was studied.

Figs. 4–6 show the variation of $CoFe_2$ alloy film thickness with current density, deposition time and bath temperature keeping other parameters constant, respectively. Initially as current density increases, film thickness increases and attains maximum thickness (3.5 μm) for 7 mA/cm^2 current density. Film thickness of about 3.5 μm is observed for 20 min deposition. Increase in bath temperature above room temperature results in decrease in film thickness due possibly to the dissolution of the film or powdery, spongy and less adherent film formation.

Table 2
Estimated deposition potentials of metals and alloy from their respective baths for different substrates and bath temperature

Sr. no.	Bath composition	Bath temperature (°C)	Deposition potential vs. SCE (volt)			
			Stainless steel	Copper	Titanium	FTO coated glass
1	0.05 M $CoSO_4$	27	−0.80	−0.77	−0.76	−0.93
2	0.1 M $FeSO_4$	27	−0.94	−1.06	−1.08	−1.06
3	(10 cc) 0.05 M $CoSO_4$ + (10cc) 0.1 M $FeSO_4$	27	−0.91	−0.88	−0.97	−1.01
4	(10 cc) 0.05 M $CoSO_4$ + (10cc) 0.1 M $FeSO_4$	50	−0.89	−0.84	−0.93	−0.99
5	(10 cc) 0.05 M $CoSO_4$ + (10cc) 0.1 M $FeSO_4$	70	−0.86	−0.81	−0.88	−0.97
6	(10 cc) 0.05 M $CoSO_4$ + (10cc) 0.1 M $FeSO_4$	90	−0.81	−0.78	−0.75	−0.94

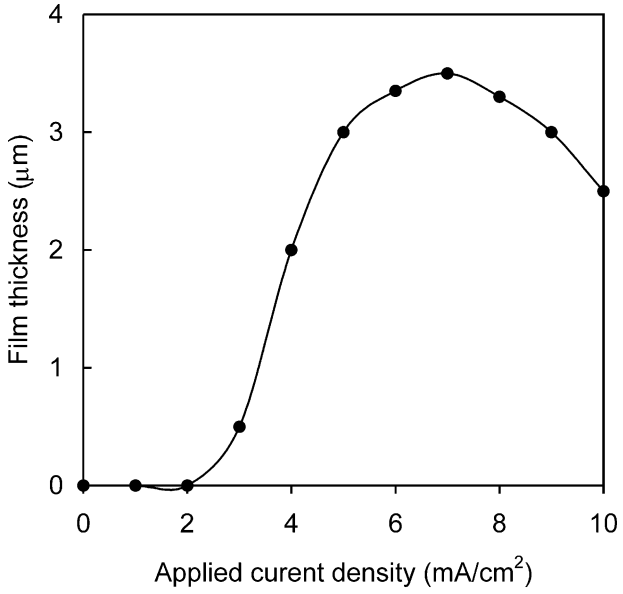

Fig. 4. Variation of film thickness with current density of $CoFe_2$ alloy deposited for 20 min at room temperature.

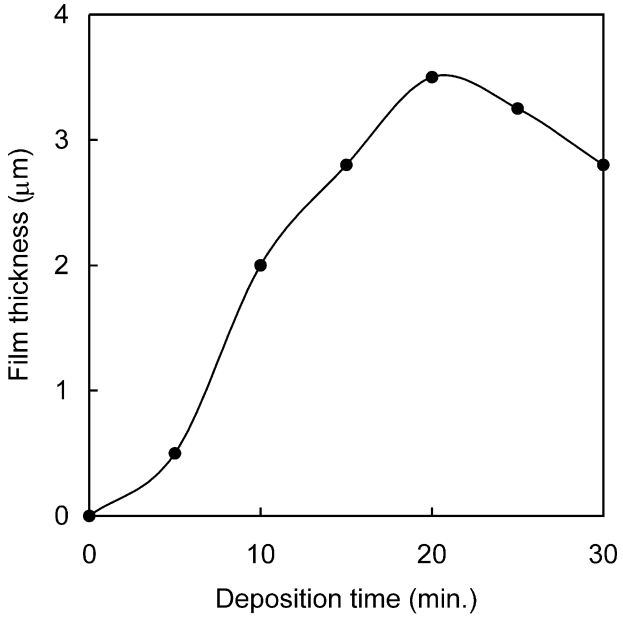

Fig. 5. Variation of film thickness with deposition time of $CoFe_2$ alloy deposited with 7 mA/cm^2 current density at room temperature.

The decrease in film thickness after deviating from the optimized processing parameters (Table 1) is due to deterioration of the film in the bath. After anodization and annealing the change in thickness is not significant and therefore alloy thickness is assumed the same for oxide films also.

3.4. Current efficiency for $CoFe_2$ alloy electrodeposition

The important factor in the electrodeposition technique is current efficiency (η) for industrial applications.

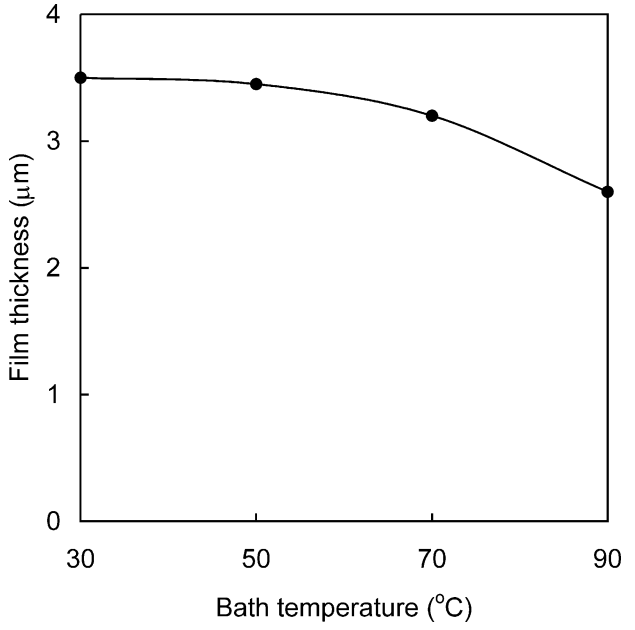

Fig. 6. Influence of bath temperature on terminal film thickness of $CoFe_2$ alloy deposited with 7 mA/cm^2 current density for 20 min.

The current efficiency was calculated by assuming the model described by Zech et al. [41]. The model is based on the assumption that both single metals are reduced in two consecutive steps and reduction of protons (H^+) and water molecules as a side reaction. In the present case, by assuming the deposited alloy has $CoFe_2$ composition and using Faraday's law, partial currents of metals were calculated. Then, the current efficiency can be calculated by summing the partial current densities of individual metallic components and dividing by the total current density. Let i_{Co} and i_{Fe} be partial current densities for Co and Fe metals, respectively. Then current efficiency is given by the following equation:

$$\eta = \frac{i_{Co} + i_{Fe}}{i_{total}} \quad (4)$$

Fig. 7 shows the variation of current efficiency with current density for $CoFe_2$ alloy deposition at room temperature for 20 min on to stainless steel substrate. Current efficiency was found to increase with increase in current density up to 7 mA/cm^2 and decreases afterwards for further increase. 80% current efficiency was found for 7 mA/cm^2 current density. Lower current efficiency below 7 mA/cm^2 current density can be attributed to decrease in the rate of deposition of metals to a point, where hydrogen evolution is the dominant reaction on the cathode [36]. Further increase in current density above 7 mA/cm^2 only leads to an increase in the rate of hydrogen evolution due to reduction of water molecules. This results in decrease in the current efficiency above 7 mA/cm^2 current density.

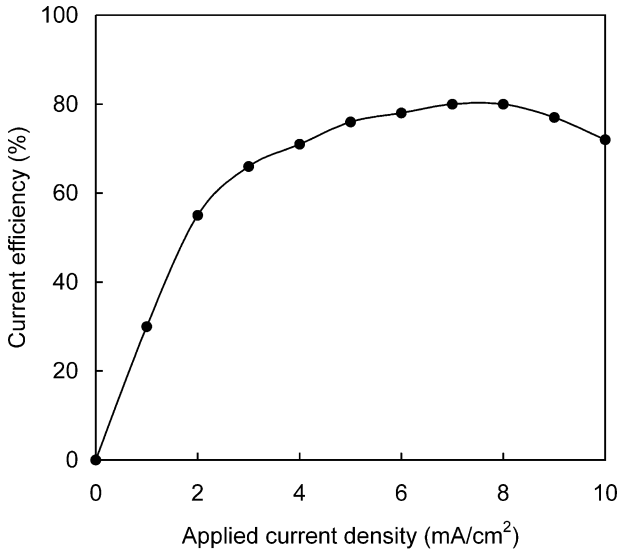

Fig. 7. Variation of current efficiency with current density of $CoFe_2$ alloy deposition for 20 min at room temperature.

The $CoFe_2$ alloy films deposited at optimized processing parameters (Table 1) were electrochemically oxidized (anodized) in 1 N KOH aqueous electrolyte and further annealed in air. Henceforth, the alloy, anodized alloy and annealed anodized alloy films will be labelled as coa_1, coa_2 and coa_3, respectively.

3.5. X-ray diffraction

X-ray diffractograms of coa_1, coa_2 and coa_3 films onto various substrates were studied. It was observed that all films are polycrystalline. The comparison (Table 3) of observed '*d*' values of coa_1, coa_2 and coa_3 films onto various substrates with standard [42] '*d*' values, suggests the formation of spinel cubic $CoFe_2O_4$ phase. Individual peaks of metal (Co and Fe) or oxides (Co–O and Fe–O) are not observed.

The inclusion of oxygen in alloy deposit may be attributed to dissolved oxygen in the presence of sulphuric acid [43]. Similar observations of oxide phase for $CuFe_2$ [24] and $NiFe_2$ [25] alloy deposited from aqueous sulphate bath have been reported earlier. Gadad and Harris [44] have studied the oxygen incorporation during electrodeposition of Ni, Fe and $NiFe_2$ alloy from simple and complex aqueous sulphate baths and reported that the oxygen content increases with increase in current density. This behaviour was corresponded to a significant increase in the pH of the solution adjacent to the electrode surface (cathode pH), which results in the

Table 3
X-ray diffraction studies of coa_1, coa_2 and coa_3 thin films onto various substrates

Substrate	Standard		Observed						Plane (hkl)	Lattice parameter 'a' (Å)			Grain size (nm)		
	'd' (Å)	I/I_o (%)	'd' (Å)			I/I_o (%)									
			coa_1	coa_2	coa_3	coa_1	coa_2	coa_3		coa_1	coa_2	coa_3	coa_1	coa_2	coa_3
Stainless steel	4.84	10	–	4.81	–	–	24	–	111	8.35	8.36	8.38	20	27	39
	2.97	30	–	–	2.97	–	–	49	220						
	2.53	100	–	2.53	2.53	–	48	100	311						
	2.09	20	2.07	–	2.08	100	–	66	400						
	1.48	40	–	–	1.48	–	–	58	440						
	1.26	4	1.27	1.27	1.27	77	100	52	622						
	1.17	2	1.16	1.16	–	36	56	–	551						
	1.09	2	1.08	1.08	–	49	32	–	701						
Copper	2.53	100	–	2.52	2.53	–	42	100	311	8.37	8.38	8.39	13	24	35
	2.09	20	2.09	2.07	2.09	100	100	51	400						
	1.28	9	–	–	1.30	–	–	26	533						
	1.17	2	1.17	1.17	–	15	30	–	551						
	1.09	2	1.09	1.09	1.09	23	15	16	731						
Titanium	2.53	100	–	2.54	2.55	–	39	80	311	8.36	8.37	8.38	17	25	29
	2.09	20	2.04	2.06	–	100	100	–	400						
	1.71	10	–	–	1.73	–	–	70	422						
	1.48	40	–	–	1.47	–	–	21	440						
	1.33	4	1.33	1.33	1.33	55	67	100	620						
	1.26	4	–	–	1.25	–	–	21	622						
	1.17	2	1.17	1.18	1.17	70	43	19	551						
FTO coated glass	2.53	100	–	–	2.54	–	–	78	311	8.37	8.38	8.39	23	27	31
	2.09	20	2.08	–	2.09	100	–	100	400						
	1.48	40	–	1.49	–	–	100	–	440						
	1.41	3	–	1.41	–	–	20	–	531						
	1.17	2	1.17	1.17	1.17	16	62	18	551						

precipitation of $M(OH)_2$ (M is depositing metal) and occlusion of this precipitate in the growing deposit. The second process by which small amount of oxygen may be incorporated in the deposit is associated with the mechanism of iron group metal deposition, which is believed to take place in two consecutive steps [34] as follows:

$$M(II) + e^- \rightarrow M(I)_{abs} \quad (5)$$

$$M(I)_{abs} + e^- \rightarrow M(s) \quad (6)$$

In these reactions, M (II) is a dissolved metal ion hydrolyzed or not, $M(I)_{ads}$ is a monovalent adsorbed reaction intermediate, which may or may not contain a hydroxyl group and M (s) is the deposited metal. If all the monovalent adsorbed reaction intermediates got released [Eq. (5)] into the solutions during the second step of the deposition process [Eq. (6)], occlusion in the growing deposit occurs.

Peaks of well defined X-ray diffraction patterns of coa_1, coa_2 and coa_3 on to various substrates were ascribed to the spinel cubic $CoFe_2O_4$ phase. Representative diffraction pattern of coa_1, coa_2 and coa_3 films onto stainless steel substrate is illustrated in Fig. 8. The differences between X-ray diffraction patterns are due only to different crystallographic orientations of the film crystallites. The observed intensities are some what different for different substrates. Since the growth conditions were identical for the films grown on to different substrates, difference in texture must be attributed to the surface morphology and preferred orientation of crystallites along different directions. After annealing, preferred orientation along (311) plane is observed, which is the same for bulk [42] spinel $CoFe_2O_4$ lattice suggesting the complete formation of spinel $CoFe_2O_4$ phase after annealing.

The calculated lattice constants of coa_1, coa_2 and coa_3 films onto various substrates are listed in Table 3. The calculated values of lattice constant are well agreed with the standard [42] lattice constant value (8.3919 Å). Increase in lattice constant after anodization and further after annealing is may be due to increase in strain in the film.

The calculated grain sizes of film material onto various substrates are listed in Table 3. The grain size of all films is in between 20–50 nm, suggesting that the films are nanocrystalline, which is the main requirement to improve the signal to noise ratio for efficient magneto-optic recording devices [45].

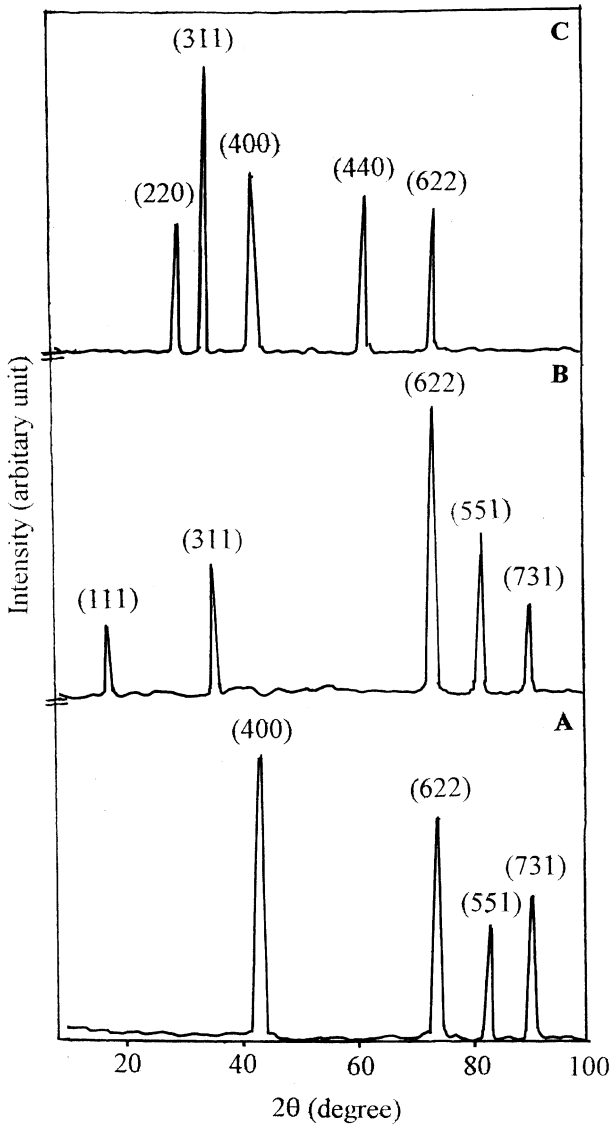

Fig. 8. Representative X-ray diffraction pattern of (A) coa_1, (B) coa_2 and (C) coa_3 films onto stainless steel substrates.

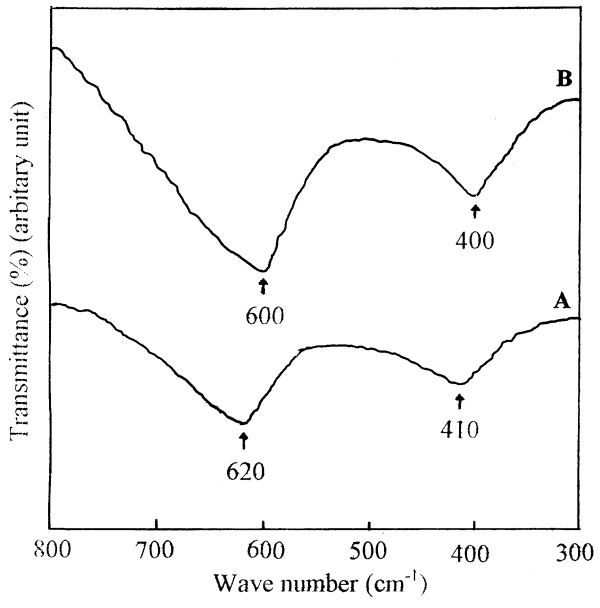

Fig. 9. IR spectra of (A) coa_2 and (B) coa_3 film powder.

3.6. IR studies

Far infrared studies on spinel type compounds is very much useful for structural investigations such as cation ordering, lattice dynamical calculations and bonding problems, e.g. bond strengths and ionicity [46]. The data relative to infrared studies of spinel oxides usually have been obtained from the transmission of the powder samples. IR spectra of (A) coa_2 and (B) coa_3 film powders are shown in Fig. 9. The spectra have been used to locate the band positions. It is observed that high frequency (ν_1) bands of powder of coa_2 and coa_3 films are at 620 and 600 cm^{-1} and low frequency (ν_2) bands are at 410 and 400 cm^{-1}, respectively, confirms the spinel structure of the films. Waldron [47] has attributed the ν_1 band to the intrinsic vibration of the tetrahedral group ($\approx$600 cm^{-1}) and ν_2 to octahedral group ($\approx$400 cm^{-1}). These bands are mainly dependent on Fe–O bond distance. From the figure, broad spectra for coa_2 and coa_3 film powders are observed. Such broadening is commonly observed for inverse spinel ferrites (MFe_2O_4). The broadening may be due to the statistical distribution of Fe at A and B site. Different spectra for coa_2 and coa_3 film powders can be attributed to particle size and shape effects [48]. The shoulder and split of bands in the IR spectrograms might be due to the presence of Jahn–Teller Fe^{2+} ions.

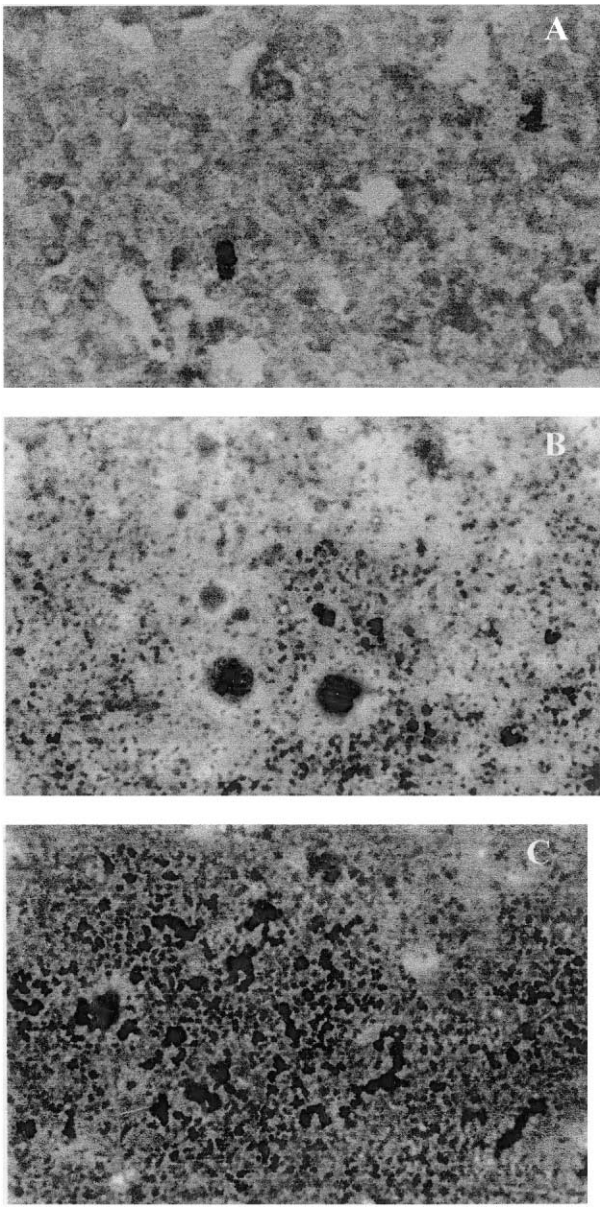

Fig. 10. Optical micrographs of (A) coa_1, (B) coa_2 and (C) coa_3 films onto FTO coated glass substrates with 160× magnification in transmission mode.

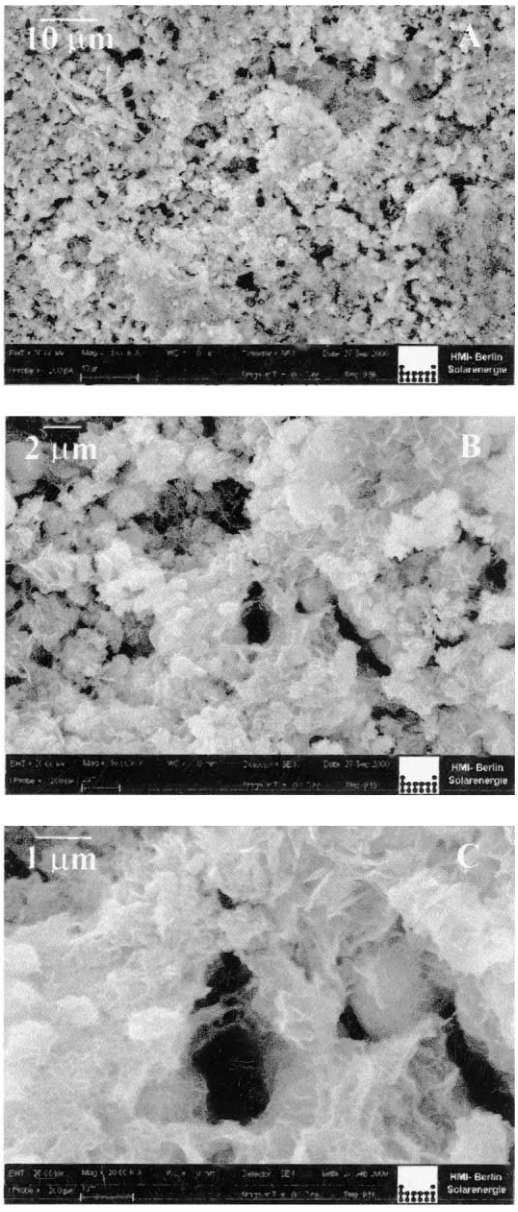

Fig. 11. Scanning electron microscopy images of coa_3 film onto stainless steel substrate with (A) 3 k× (B) 10 k× and (C) 30 k× magnifications.

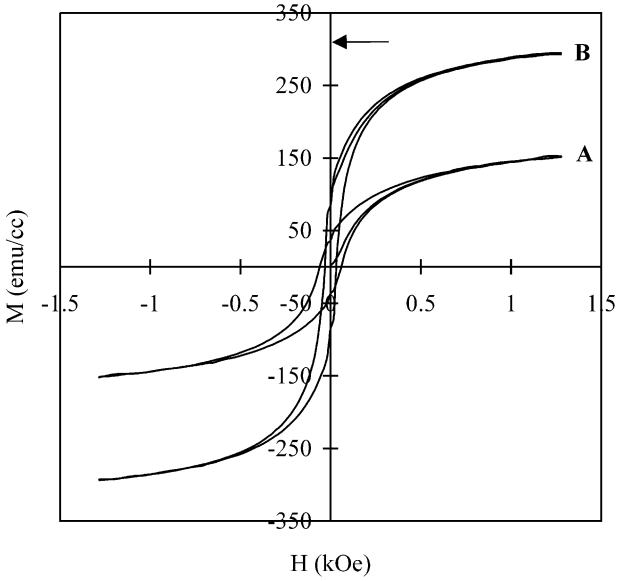

Fig. 12. M–H loops of (A) coa_2 and (B) coa_3 films onto copper substrates at room temperature (27 °C). The bulk saturation magnetization (Ms = 308 emu/cc) is shown by the arrow.

3.7. Surface morphology and microstructure

Fig. 10 shows optical micrographs of (A) coa_1, (B) coa_2 and (C) coa_3 films onto FTO coated glass substrates with 160 × magnification in transmission mode. The films have smooth, uniform and dense surface. The anodized film shows compact intergrain spacing and improvement in grain size. Further compact surface and improved grain size is observed after annealing.

Fig. 11 shows the scanning electron microscopy images of etched coa_3 film onto stainless steel substrates with different magnifications: (A) 3 k×, (B) 10 k× and (C) 30 k×. The films have crack free and uniform surface at lower as well as higher magnifications.

3.8. Magnetic properties

Fig. 12 shows M–H loops of (A) coa_2 and (B) coa_3 films onto copper substrates. The arrow in the figure shows the value of saturation magnetization of bulk $CoFe_2O_4$ prepared by a standard ceramic method [49]. The values of saturation magnetization (Ms), residual magnetization (Mr) and coercive force (Hc) are determined from the loops and listed in Table 4. The increase in values of Ms, Mr and Hc after annealing is may be due to increase in grain size, decrease in surface layer effects and change in cation distribution. The magnetic properties of annealed films are comparable to the bulk properties [49].

Table 4
Magnetic properties of coa_2 and coa_3 films on to copper substrates at room temperature. The magnetic field was applied in plane of the film

Film	Ms (emu/cc)	Mr (emu/cc)	He (kOe)
coa_2	151	36	0.03
coa_3	293	104	0.05

4. Conclusions

Nanocrystalline spinel cubic $CoFe_2O_4$ thin films have been successfully deposited on to various conducting substrates using novel electrochemical route. Optimized preparative parameters give $CoFe_2$ alloy films with thickness about 3.5 μm and 85% current efficiency. Observation of oxide phase for $CoFe_2$ alloy has been attributed to the dissolved oxygen in the bath and increase in the pH of the solution adjacent to the cathode surface which results into the precipitation of $M(OH)_2$ and their occlusion in the depositing material. Effect of anodization and annealing leads to the change of crystallographic texture and increase in grain size. After annealing preferred orientation along (311) plane is observed which suggests the complete formation of the spinel $CoFe_2O_4$ phase. IR absorption studies confirm the spinel structure of the oxide films. Annealed films have magnetic properties comparable to the bulk $CoFe_2O_4$.

Acknowledgements

Thanks are due to Dr. Alok Banerjee and Mr. Sunil Nair, Inter-University Consortium for DAE Facilities, Indore, India for their help in VSM characterizations.

References

[1] G.D. Rieck, J.J.M. Thijssen, Acta Crystallogr. B24 (1968) 982.
[2] G.A. Sawatzky, F. Van der Woude, A.H. Morrish, J. Appl. Phys. 39 (1968) 1204.
[3] K.C. Patil, S. Sundar Manoharan, D. Gajapathy, in: N.P. Cheremisinoff (Ed.), Handbook of Ceramics and Composites, Vol.1 Synthesis and Properties, Marcel Dekker Inc., New York, 1990, p. 469.
[4] V.S. Darshane, S.S. Lokegaonkar, S.G. Oak, J. Phys. IV France 7 (1997) C1–683.
[5] F. Bodker, S. Morup, S. Linderoth, Phys. Rev. Lett. 72 (1994) 282.
[6] Y. Tamara, M. Kojima, N. Hasegawa, M. Tsuji, K. Ehrensberger, A. Steinfeld, J. Phys. IV France 7 (1997) C1-673.
[7] M. Abe, T. Itoh, Y. Tamaura, Thin Solid Films 216 (1992) 155.
[8] C.V. Gopal Reddy, S.V. Manorama, V.J. Rao, J. Mater. Sci. Lett. 19 (2000) 775.
[9] R.K. Ahrenkiel, T.J. Coburn, IEEE Trans. Magn. 11 (1975) 1103.
[10] J.W.D. Martens, W.L. Peeters, H.M. Van Noort, M. Errnan, J. Phys. Chem. Solids 46 (1985) 411.
[11] K. Suzuki, T. Namikawa, T. Yamazaki, Jpn. J. Appl. Phys. 27 (1988) 361.
[12] S.N. Okuno, S. Hashimoto, K. Inomata, J. Appl. Phys. 71 (1992) 5926.
[13] R. Valenzuela, Magnetic Ceramics, Cambridge University Press, Cambridge, 1994.

[14] P.C. Dorsey, P. Lubitz, D.B. Chrisey, J.S. Horowitz, J. Appl. Phys. 79 (1996) 6338.
[15] J.A. Na, J. Appl. Phys. 79 (1996) 4893.
[16] D.M. Schleich, Y. Zhang, Mater. Res. Bull. 30 (1995) 447.
[17] J. Lee, J.Y. Park, Y. Oh, C.S. Kim, J. Appl. Phys. 84 (1998) 2801.
[18] S.S. Bellad, C.D. Lokhande, C.H. Bhosale, Ind. J. Pure Appl. Phys. 35 (1997) 565.
[19] E.S. Murdock, R.F. Simmons, R. Davidson, IEEE Trans. Magn. 28 (1992) 3078.
[20] M. Abe, Y. Tamaura, Jpn. J. Appl. Phys. Lett. 22 (1983) 511.
[21] M. Abe, Y. Tamaura, J. Appl. Phys. 55 (1984) 2614.
[22] V. Surve, V. Puri, Bull. Electrochem. 14 (1998) 151.
[23] J.C. Grenier, A. Wattiaux, L. Fournes, M. Pouchard, J. Etourneau, J. Phys. IV France 7 (1997) C1–49.
[24] S.D. Sartale, C.D. Lokhande, Mater Chem. Phys. 70 (2001) 274.
[25] S.D. Sartale, C.D. Lokhande, Ind. J. Eng. Mater. Sci. 7 (2000) 404.
[26] S.S. Djokic, J. Electrochem. Soc. 146 (1999) 1824.
[27] R.K. Pandey, S.N. Sahu, S. Chandra, Handbook of Semiconductor Electrodeposition, Marcel Dekker, Inc, New York, 1996.
[28] A. Brenner, Electrodeposition of Alloys, Vols. 1 and 2, Academic Press, New York, 1963.
[29] S.S. Djokic, in: B.E. Conway, G. Jerkiewicz (Eds.), Electrochemistry and Materials Science of Cathodic Hydrogen Absorption and Adsorption, The Electrochemical Society Proceedings Series, Pennington, NJ, 1994, p. 245.
[30] H. Dahms, I.M. Croll, J. Electrochem. Soc. 112 (1965) 771.
[31] H. Venkatasetty, J. Electrochem. Soc. 117 (1970) 403.
[32] L.B. Harris, J. Electrochem. Soc. 120 (1973) 1034.
[33] J. Horkans, J. Electrochem. Soc. 126 (1979) 1861.
[34] M. Matlosz, J. Electrochem. Soc. 140 (1993) 2272.
[35] B.C. Baker, A.C. West, J. Electrochem. Soc. 144 (1997) 169.
[36] K. Sasaki, J.B. Talbot, J. Electrochem. Soc. 145 (1998) 81.
[37] N. Zech, E.J. Podlaha, D. Landolt, J. Electrochem. Soc. 146 (1999) 2886.
[38] D.R. Lide (Ed.), CRC Hand Book of Chemistry and Physics, 79th Edn, CRC Press, Boca Raton, FL, 1998–1999.
[39] C.D. Lokhande, S.H. Pawar, J. Phys. D: Appl. Phys. 20 (1987) 7213.
[40] W. Blum, G.B. Megaboom, Principles of Electroplating and Electroforming, McGraw Hill Publishing Company Ltd, India, 1930.
[41] N. Zech, E.J. Podlaha, D. Landolt, J. Electrochem. Soc. 146 (1999) 2892.
[42] JCPDS–ICDD (1994) Card No: 22-1086.
[43] S.G. Ellis, J. Appl. Phys. 38 (1967) 2906.
[44] S. Gadad, T.M. Harris, J. Electrochem. Soc. 145 (1998) 3699.
[45] S. Koutani, G. Gavoille, J. Magn. Magn. Mater. 138 (1994) 237.
[46] M. Lenglet, F. Hochu, Mater. Res. Bull. 32 (1997) 863.
[47] R.D. Waldron, Phys. Rev. 99 (1955) 1727.
[48] J. Preudhomme, P. Tarte, Spectrochim Acta 27A (1971) 1817.
[49] P.N. Vasambekar, C.B. Kolekar, A.S. Vaingankar, Mater. Chem. Phys. 60 (1999) 282.